



## Models of neurovascular coupling via potassium and EET signalling

Hannah Farr<sup>a,b</sup>, Tim David<sup>a,\*</sup>

<sup>a</sup> Centre for Bioengineering, University of Canterbury, New Zealand

<sup>b</sup> Van der Veer Institute for Parkinson's and Brain Research, Christchurch, New Zealand

### ARTICLE INFO

#### Article history:

Received 11 February 2011

Received in revised form

8 July 2011

Accepted 11 July 2011

Available online 20 July 2011

#### Keywords:

Neurovascular coupling

Cerebral blood flow regulation

Potassium buffering

### ABSTRACT

Functional hyperemia is an important metabolic autoregulation mechanism by which increased neuronal activity is matched by a rapid and regional increase in blood supply. This mechanism is facilitated by a process known as “neurovascular coupling”—the orchestrated communication system involving neurons, astrocytes and arterioles. Important steps in this process are the production of EETs in the astrocyte and the release of potassium, via two potassium channels (BK and KIR), into the perivascular space. We provide a model which successfully accounts for several observations seen in experiment. The model is capable of simulating the approximate 15% arteriolar dilation caused by a 60-s neuronal activation (modelled as a release of potassium and glutamate into the synaptic cleft). This model also successfully emulates the paradoxical experimental finding that vasoconstriction follows vasodilation when the astrocytic calcium concentration (or perivascular potassium concentration) is increased further. We suggest that the interaction of the changing smooth muscle cell membrane potential and the changing potassium-dependent resting potential of the KIR channel are responsible for this effect. Finally, we demonstrate that a well-controlled mechanism of potassium buffering is potentially important for successful neurovascular coupling.

© 2011 Elsevier Ltd. All rights reserved.

### 1. Introduction

Arteries within the brain are known to regulate their blood supply in response to local changes, such as tissue metabolic activity, by several autoregulation mechanisms. A non-dimensional representation of autoregulation coupled with an asymmetric binary tree algorithm (approx 1,000,000 vessel segments) simulating the cerebrovasculature has been developed by David et al. (2009). This model incorporates the known myogenic (pressure) and wall shear stress autoregulatory responses, but currently only incorporates a phenomenological model of the metabolic autoregulatory responses. The need for a physiologically correct model that attempts to incorporate the complex chemical pathways underlying metabolic autoregulation prompted an investigation into the specific ion transports and cell apparatus involved. These investigations have highlighted the importance of a phenomenon known as functional hyperemia, a mechanism by which increased neuronal activity is matched by a rapid and regional increase in blood supply. Having a clear understanding of functional hyperemia is vital for fMRI imaging and neurological disease research (Iadecola, 2004; Xu et al., 2007). It is therefore surprising that the major pathways that control functional hyperemia have only

recently been elucidated (Attwell et al., 2010). Functional hyperemia is now recognised as being achieved through “neurovascular coupling”, the intercellular communication system between cells comprising the neurovascular unit (neurons, astrocytes and microvessels). The delivery of a request for increased nutrients from neuron to arteriole is facilitated by chemical processes that occur in the astrocyte, a star-shaped glial cell with processes that surround both synapses and arterioles (Filosa and Blanco, 2007).

There have been many possible astrocyte-derived vasoactive signals identified, including NO, ATP and arachidonic acid (AA) metabolites (such as epoxyeicosatrienoic acids (EETs)) (Girouard and Iadecola, 2006). Numerous studies have also documented that increases in extracellular potassium concentration ( $[K^+]$ ) can lead to vasodilation (and in higher concentrations, vasoconstriction) (McCarron and Halpern, 1990; Cameron and Caronna, 1976; Kuschinsky et al., 1972; Golding et al., 2000; Edwards et al., 1988). Further studies by Filosa et al. (2006) and others (Chrisobolis et al., 2000; Nakahata et al., 2006; Johnson et al., 1998; Knot et al., 1996) have proposed that the release of  $K^+$  ions from astrocyte endfeet and the subsequent activation of KIR channels on vascular smooth muscle cells (SMCs) comprises a rapid mechanism of arteriolar dilation. There has long been an argument for chemical versus electrical signalling in neurovascular coupling, and it has still not been determined if it is these biochemical signals that modulate arteriolar diameter and hence blood flow, or if it is the “electric” signal in the form of a flux (current) of positive  $K^+$  ions.

\* Corresponding author.

E-mail address: [tim.david@canterbury.ac.nz](mailto:tim.david@canterbury.ac.nz) (T. David).

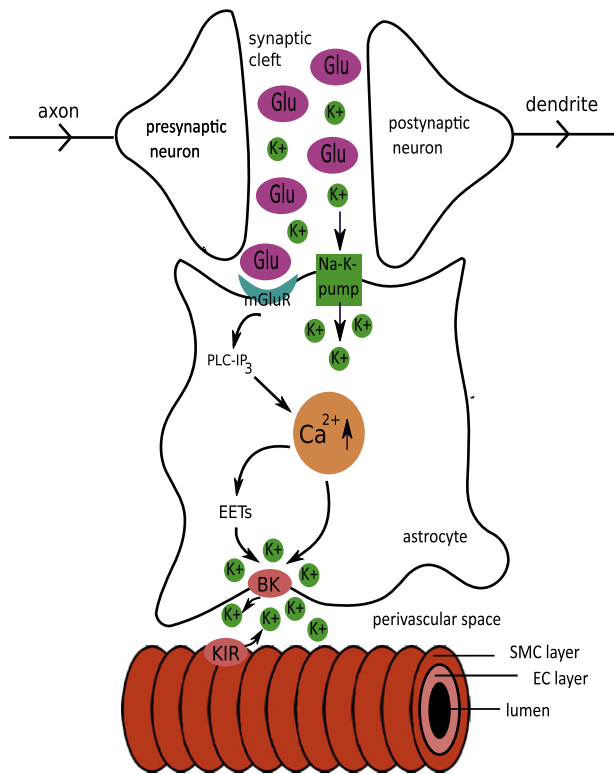


Fig. 1. Neurovascular coupling: an overview.

Filosa and Blanco (2007) suggest that both of these mechanisms coexist and interact, with the chemical signals being better suited to maintain changes in vessel tone in response to sustained neuronal activation and  $K^+$  fluxes being more appropriate for eliciting the rapid response following the onset of neuronal activation. In keeping with these hypotheses we include aspects of both these signals in the form of  $K^+$  fluxes and EET release.

It is important at this point to make a distinction between the mechanism known as “ $K^+$  siphoning” and the mechanism that we are proposing. The “ $K^+$  siphoning” hypothesis states that  $K^+$  released from active neurons depolarises astrocytes, leading to  $K^+$  efflux from astrocyte endfeet (Paulson and Newman, 1987). This mechanism of neurovascular coupling has been tested by depolarising astrocytes while measuring blood vessel diameter (Metea et al., 2007). Depolarisation fails to dilate blood vessels, proving that  $K^+$  siphoning does not contribute to vasodilation. In our mechanism,  $K^+$  is pumped into the astrocyte via the Na–K pump (causing an overall depolarisation), but is released by endfoot BK channels due to the action of EETs on them, not due to the depolarising membrane. Therefore, we have two independent mechanisms controlling the influx and efflux of potassium in our model astrocytes.

We present here a model of the entire neurovascular unit, including the synaptic space, astrocyte, and both active layers of the arteriole (smooth muscle cells (SMCs) and endothelial cells (ECs)) using the work of Filosa et al. (2006) as a guide. This is the first mathematical model of potassium signalling in a complete neurovascular unit. There have been several models produced of sections of the neurovascular unit, and we extend and adapt some of these. We use the models of Koenigsberger et al. (2006) for our coupled EC and SMC layers of the arteriole, with extensions to include the KIR channels needed as part of our model. The neurovascular unit model of Bennett et al. (2008) includes only the EET mechanisms, and both Koenigsberger et al. (2006) and

Bennett et al. (2008) use simplistic (first order or proportional) models of muscle contraction. We therefore use only the astrocyte equations of Bennett et al. (2008), extending them to include potassium signalling. Unlike Bennett et al. (2008), we assume that the astrocyte-derived EETs do not diffuse through the perivascular space to the arteriole, but act primarily upon the BK channels at the astrocytic endfeet. It is possible that EETs or other AA-derived metabolites act on the SMCs themselves (Attwell et al., 2010), but we assume, in keeping with the findings of Higashimori et al. (2010), that EETs act directly on astrocytic endfeet and in turn modulate  $Ca^{2+}$  levels and  $K^+$  currents in an autocrine manner. Finally, we further develop a contraction model, using Kudryashov and Chernyavskii (2008) to produce a more physiologically correct model that takes into account the multilayer structure of the arterial wall, and the nonlinear viscoelastic properties of the wall material. Furthermore, in contrast to other autoregulation models (Bennett et al., 2008; Gonzalez-Fernandez and Ermentrout, 1994) who consider only the dynamics in the SMC component of the wall; we include a coupled SMC and EC endothelial cell layer. We do not consider endothelium-dependent vasomodulatory mechanisms at this stage, but have developed this model so that these mechanisms can be added at a later date.

## 2. Theory

### 2.1. Overview of the model

The presented model includes all major mechanisms that occur in the neurovascular coupling process as proposed by Filosa and Blanco (2007), starting with the release of glutamate at the synapse due to neural activity and ending with the dilation of an arteriolar segment. Fig. 1 shows the major cells and processes involved. They are modelled as follows: (1) neural activity causes the release of potassium and glutamate into the synaptic space; (2) potassium is taken into the astrocytic cytosol via the Na–K pump, while glutamate binds to metabotropic receptors on the top “arm” of the astrocyte leading to the release of  $IP_3$  into the cytosol of the astrocyte; (3)  $IP_3$  stimulates the release of calcium from intracellular stores via PLC, causing a rise in cytosolic calcium. AA-derived EETs are also produced due to this rise in calcium; (4) both EETs and increase in cytosolic calcium gate the “BK” potassium channels that are present in the endfeet of the astrocyte causing a release of potassium into the perivascular space between the smooth muscle cells surrounding the arteriole and the endfoot; (5) the rise in potassium in the perivascular space further gates the “KIR” potassium channels in the smooth muscle cells (SMCs), causing them to open, extruding further potassium into this perivascular space, hyperpolarising the SMC membrane in doing so; (6) this hyperpolarisation closes voltage operated calcium channels in the SMCs, preventing the influx of  $Ca^{2+}$ ; (7) the decreased SMC cytosolic calcium then mediates the dilation of the arteriole through the consequent detachment of myosin–actin cross-bridges and relaxation of smooth muscle.

During the neurovascular coupling process described above, potassium accumulates within the perivascular space, and is removed by a process known as “potassium buffering” (Chen and Nicholson, 2000). To properly develop a model of potassium buffering, an interacting network of neurovascular units would need to be established. We therefore do not attempt to model potassium buffering at this time, but instead look only at the uptake of potassium from the synaptic cleft and the extrusion of potassium into the perivascular space.

Diffusion processes are known to occur as a part of neurovascular coupling, in particular, calcium increases are known to propagate down from the synaptic end of the astrocyte to the endfeet as a “calcium wave”. We do not, however, consider a spatial distribution of chemical species throughout any of the cells, rather, we adopt a lumped parameter approach, and model each cell as a well-mixed compartment.

## 2.2. Potassium in the synaptic space

We adopt a very simple model for the concentration of potassium in the synaptic space. Potassium is released into this space by the neurons only during neuronal activation, and is constantly removed from the space via the Na–K pump positioned on the top “arm” of the astrocyte. The smooth “pulse” of potassium release during neuronal activation is represented by  $J_{K_s}$ , and the Na–K pump flux is denoted by  $J_{NaK_s}$ . The concentration of potassium in the synaptic cleft is therefore the difference of these two fluxes, as

$$\frac{dK_s}{dt} = J_{K_s} - J_{NaK_s} \quad (1)$$

$J_{NaK_s}$  is taken from (Østby et al., 2009)

$$J_{NaK_s} = J_{NaK_{max}} \left( \frac{K_s}{K_s + K K O_a} \right) \left( \frac{N a i_a^{1.5}}{N a i_a^{1.5} + K N a i_a^{1.5}} \right) \quad (2)$$

$J_{NaK_{max}}$  is the maximum pump flux and  $K K O_a$  and  $K N a i_a$  are the threshold values for  $[K^+]_i$  and  $[Na^+]_i$ , respectively.  $N a i_a$  (the intercellular sodium concentration) is assumed to be constant for simplicity.

## 2.3. Astrocyte

Voltage operated calcium channels (VOCCs) are expressed in cultured astrocytes, and Filosa and Blanco (2007) include these channels as an important entity in their hypothesised process of neurovascular coupling. However, Carmignoto et al. (1998) show that VOCCs may not necessarily be responsible for the propagating calcium waves involved as part of neurovascular coupling. We therefore exclude these channels in this model. We do, however, include a general “leak” term. The equations and parameters for the leak current are those of Gonzalez-Fernandez and Ermentrout (1994).

The voltage- and calcium-operated potassium channel (BK) and the “inwardly rectifying” potassium and voltage gated potassium channel (KIR) are both expressed in astrocyte processes surrounding synapses and arterioles (Price et al., 2002; Higashi et al., 2001). However, according to Zhou and Kimelberg (2000), astrocytes can be divided into two classes: variably rectifying astrocytes (VRA) and outwardly rectifying astrocytes (ORA), where only VRA seem suited for uptake of extracellular potassium via KIR channels. We assume then that ORA are therefore responsible for “pushing” potassium out via BK channels, and VRA for “pulling” it back in again via KIR channels, and together they cooperate to move potassium in and out of extracellular spaces (potassium buffering). As we are not investigating the process of potassium buffering at this time, we will look only at the ORA, and as such will only include the BK channels in the astrocyte.

The foundation for this model of the astrocyte cell processes follows that of Bennett et al. (2008). We further develop their equations, with additions and adaptations to include a differential equation for the astrocyte membrane voltage, which includes ohmic relationships for BK and leak fluxes. The BK channel flux is modelled from Gonzalez-Fernandez and Ermentrout (1994), with a voltage shift term that is dependent on the EET concentration.

The differential equations describing the dynamics in the astrocyte are as follows. Here  $c_k$  is the cytosolic  $Ca^{2+}$  concentration,  $v_k$  is the membrane voltage,  $s_k$  is the concentration of  $Ca^{2+}$  in the endoplasmic reticulum (ER),  $h_k$  is the inactivation variable for  $IP_3$ ,  $i_k$  is the concentration of  $IP_3$  and  $eet_k$  is the concentration of EETs.

Calcium moves between the cytosol and the endoplasmic reticulum (ER), and the cytosol and the extracellular space surrounding the astrocyte, by several mechanisms. We denote the calcium flux from the ER to the cytosolic volume through  $IP_3$  receptors ( $IP_3R$ ) by  $J_{IP_3}$ , the leakage flux from the ER to the cytosol as  $J_{ER_{leak}}$  and the ATP-dependent pump flux from cytoplasm to ER as  $J_{pump}$ . Thus we can write

$$\frac{dc_k}{dt} = B_{cyt} (J_{IP_3} - J_{pump} + J_{ER_{leak}}) \quad (3)$$

The constant  $B_{cyt}$  is a steady state approximation for buffering in the cytosol (Bennett et al., 2008).

The astrocyte membrane voltage changes due to fluxes of ions leaving the astrocyte, namely: the potassium flux through BK channels ( $J_{BK_k}$ ) and a general leak flux ( $J_{leak_k}$ —not to be confused with  $J_{ER_{leak}}$ ). We therefore can state the relationship:

$$\frac{dv_k}{dt} = \frac{1}{C_{ast}} (-J_{BK_k} - J_{leak_k} + J_{NaK_s}) \quad (4)$$

where  $C_{ast}$  is the astrocyte cell membrane capacitance.

$s_k$ , the concentration of calcium in the ER, was assumed to be constant in the original model (Bennett et al., 2008). In order to investigate this variable further, we incorporate the following differential equation:

$$\frac{ds_k}{dt} = \frac{-1}{VR_{ER_{cyt}}} \left( \frac{dc_k}{dt} \right) \quad (5)$$

where  $VR_{ER_{cyt}}$  is the ratio of ER (stores) volume to cytosolic volume.

The flux  $J_{IP_3}$  is written as

$$J_{IP_3} = J_{max} \left[ \left( \frac{i_k}{i_k + K_I} \right) \left( \frac{c_k}{c_k + K_{act}} \right) h_k \right]^3 \times \left[ 1 - \frac{c_k}{s_k} \right] \quad (6)$$

$J_{max}$  is the maximum rate,  $K_I$  is the dissociation constant for  $IP_3$  binding to an  $IP_3R$  and  $K_{act}$  is the dissociation constant for  $Ca^{2+}$  binding to an activation site on an  $IP_3R$ . The inactivation variable  $h_k$  (which denotes the action of  $IP_3R$  that have not been inactivated by  $Ca^{2+}$ ) is modelled as a dynamic variable:

$$\frac{dh_k}{dt} = k_{on} [K_{inh} - (c_k + K_{inh}) h_k] \quad (7)$$

Here  $k_{on}$  is the rate of  $Ca^{2+}$  binding to the inhibitory site on the  $IP_3R$  and  $K_{inh}$  is the corresponding dissociation constant.  $J_{ER_{leak}}$  is determined by

$$J_{ER_{leak}} = P_L \left( 1 - \frac{c_k}{s_k} \right) \quad (8)$$

where  $P_L$  is determined from the steady state calcium balance, and  $J_{pump}$  is

$$J_{pump} = V_{max} \frac{c_k^2}{c_k^2 + k_{pump}^2} \quad (9)$$

$V_{max}$  is the maximum pumping rate and  $k_{pump}$  is the dissociation constant. For  $IP_3$ , we have

$$\frac{di_k}{dt} = r_h G - k_{deg} i_k \quad (10)$$

where  $r_h$  is the maximum rate of  $IP_3$  production in astrocyte due to glutamate attachment at metabotropic receptors,  $k_{deg}$  is the rate constant for  $IP_3$  degradation in astrocyte, and  $G$  is the ratio of

active G-protein to total G-protein, and satisfies

$$G = \frac{\rho + \delta}{K_G + \rho + \delta} \quad (11)$$

$\rho$  is the ratio of bound to total glutamate receptors on the synapse end of the astrocyte, and  $K_G$  is the G-protein dissociation constant.  $\delta$  is the ratio of the activities of the unbound and bound receptors. The inclusion of  $\delta$  allows for there to be background activity even in the absence of ligand binding (i.e. unbound receptors can still activate a small amount of G-protein). This behaviour is more fully described in the work of Lemon et al. (2003).

Finally,  $\text{Ca}^{2+}$ -dependent EET production is described with the simple relationship:

$$\frac{deet_k}{dt} = V_{eet}(c_k - c_{k,min}) - k_{eet}eet_k \quad (12)$$

$c_{k,min}$  is the minimum  $\text{Ca}^{2+}$  concentration required for EET production.  $V_{eet}$  and  $k_{eet}$  are the rate constants for EET production and EET degradation, respectively, where degradation is assumed to follow the first-order kinetics.

### 2.3.1. "Leak" channel models

The relationship for  $J_{leak_k}$  is taken from (Gonzalez-Fernandez and Ermentrout, 1994)

$$J_{leak_k} = g_{leak_k}(v_k - v_{leak_k}) \quad (13)$$

Here  $g_{leak_k}$  and  $v_{leak_k}$  are considered to be constant.

### 2.3.2. BK channel model

$J_{BK_k}$  in Eq. (4) can be described by the ohmic relationship:

$$J_{BK_k} = g_{BK_k}n(v_k - v_{BK_k}) \quad (14)$$

where  $g_{BK_k}$  is the conductance,  $v_{BK_k}$  is the Nernst reversal potential and  $n$  is the open BK channel probability.

BK channel equations are taken from Gonzalez-Fernandez and Ermentrout (1994). Work by Lu et al. (2001) shows that both EETs and EET-derived dihydroxyeicosatrienoic acids (DHETs) act as potent activators of BK channels, where DHETs were shown to shift the voltage at which the channel open probability was half-maximal. We therefore incorporate a EET-dependent voltage shift ( $eet_{shift}$ ) into the relationship given by Gonzalez-Fernandez and Ermentrout (1994), to get  $n_\infty$ , the equilibrium distribution of openings for the BK channel:

$$n_\infty = 0.5 \left( 1 + \tanh \left( \frac{(v + eet_{shift}eet_k) - v_3}{v_4} \right) \right) \quad (15)$$

The time course of the fraction of BK channel open states,  $n$ , is described, after Morris and Lecar (1981), by the first-order kinetics of opening:

$$\frac{dn}{dt} = \phi_n(n_\infty - n) \quad (16)$$

where the time constant associated with the opening of these channels,  $\phi_n$ , is based on statistical considerations (Ehrenstein and Lecar, 1977):

$$\phi_n = \psi_n \cosh \left( \frac{v_k - v_3}{2v_4} \right) \quad (17)$$

$$v_3 = -\frac{v_5}{2} \tanh \left( \frac{c_k - Ca_3}{Ca_4} \right) + v_6 \quad (18)$$

In this case,  $\psi_n$  is a characteristic time and  $v_3$  incorporates a calcium-dependent shift on the distribution of BK channel open states with respect to membrane voltage.  $v_3$  is the voltage associated with the opening of half the population and  $v_4$  is a measure of the spread of the distribution.  $v_5$  determines the range of the shift of  $n_\infty$ , as calcium varies.

## 2.4. Potassium in the perivascular space

We adopt a simple model for the concentration of potassium in this perivascular space at this stage—assuming that the accumulating potassium is removed by a potassium-dependent decay term. Potassium enters the perivascular space via astrocyte BK channels and SMC KIR channels, with corresponding fluxes denoted by  $J_{BK_k}$  and  $J_{KIR_k}$ , respectively. The balance of these fluxes, along with the decay term, gives the following differential equation:

$$\frac{dk_p}{dt} = \frac{1}{VR_{pa}}(J_{BK_k}) + \frac{1}{VR_{ps}}(J_{KIR_k}) - R_{decay}(k_p - k_{p,min}) \quad (19)$$

Here  $VR_{pa}$  and  $VR_{ps}$  are the volume ratios of perivascular space to astrocyte and to SMC, respectively.  $R_{decay}$  is the estimated potassium clearance rate from the extracellular space and  $k_{p,min}$  is the equilibrium potassium concentration in the perivascular space.

## 2.5. Smooth muscle and endothelial cells

The foundation for this model of the smooth muscle and endothelial cell processes follows that of Koenigsberger et al. (2006). We add a KIR channel flux in the SMCs, which is modelled similarly to that of the BK potassium channels described above. We therefore use the following equation for the time course of the fraction of open KIR channel states,  $k$ :

$$\frac{dk}{dt} = \frac{1}{\tau}(k_\infty - k) \quad (20)$$

Again,  $\tau$  is the time constant associated with the opening of these channels and  $k_\infty$  is the equilibrium distribution of open states.

$J_{KIR_k}$  is incorporated into the SMC voltage differential equation in the following form:

$$J_{KIR_k} = g_{KIR_k}k(v_i - v_{KIR}) \quad (21)$$

Again, here  $g_{KIR}$  is the membrane conductance for the inwardly rectifying potassium current and  $v_{KIR}$  is the corresponding Nernst reversal potential.

Patch clamp experiments by Kurachi (1985) give a kinetic model for the activation gate of the KIR channel. The time constant associated with the change in the fraction of the open channels ( $\tau$ ) is the "balance" of the two opening and closing constants,  $\alpha$  and  $\beta$ :

$$\tau = \frac{1}{\alpha + \beta} \quad (22)$$

with

$$\alpha = \frac{1020}{1 + \exp \left( \frac{v_i + 18}{6.8} \right)} \quad (23)$$

$$\beta = 26.9 \exp(0.06(v_i + 18)) \quad (24)$$

where  $v_i$  is the membrane potential minus  $v_{KIR}$  (the reversal potential).

The equilibrium open channel probability is given by the (sigmoidal) relation:

$$k_\infty = \frac{\alpha}{\alpha + \beta} \quad (25)$$

$v_{KIR}$  (the Nernst reversal potential for the KIR channel) increases with  $[K^+]_0$  (the perivascular potassium concentration). Using the data from Quayle et al. (1997), and assuming a linear relationship in this  $[K^+]_0$  range, we obtain

$$v_{KIR_k} = 57 \log_{10}[K^+]_0 - 130 \quad (26)$$

Finally, Quayle et al. (1996) give the changes in inward rectifier conductance with changes in  $[K^+]_0$ :

$$g_{KIR} = 145 \sqrt{[K^+]_0} \quad (27)$$

where conductance is given in pS and  $[K^+]_0$  is in mM. KIR channels (at least in the coronary circulation) are expressed at a higher density (up to 50 times higher) in small diameter arteries than in large ones (Quayle et al., 1996). In this model, we are interested primarily in the very small precapillary arterioles and we therefore assume a conductance value 50 times than that given.

We similarly make an amendment to the conductance for the stretch- (or pressure-) activated ion channel. It is given by Koenigsberger et al. (2006) as a model estimation of  $0.0061 \mu\text{M mV}^{-1} \text{s}^{-1}$ . The stretch-activated channel conductance of a SMC from a resistance sized artery in the rat mesentery (Setoguchi et al., 1997) is approximately 2.5 times that given by Koenigsberger et al. (2006). We believe it is possible that a variable distribution of stretch-activated channels exists up and down the branches of a vascular tree (just as it does for KIR channels). We therefore set the stretch-activated channel conductance to a higher value of  $0.46 \mu\text{M mV}^{-1} \text{s}^{-1}$  so as to give a SMC resting potential close to that in the pressurised arterioles measured by Nystoriak et al. (2011).

## 2.6. Muscle mechanics model

Equations describing the motion of the arterial wall are modified from the model of Kudryashov and Chernyavskii (2008).

Consider a viscoelastic arteriolar wall element of mass  $\Delta m$ , density  $\rho_w$ , thickness  $h$ , radius  $R$ , and length  $\Delta x$ . The two forces acting on the wall are  $f_r$ , a force proportional to the tangential stress tensor,  $\sigma_{\theta\theta}$ , and  $f_p$  the force exerted by blood pressure. These are given by Eqs. (28) and (29), respectively,

$$f_r = -\sigma_{\theta\theta} 2\pi h_0 \Delta x \quad (28)$$

$$f_p = \Delta p 2\pi R \Delta x \quad (29)$$

where  $\Delta p$  is the transmural pressure.  $R_0$  and  $h_0$  are defined as the basal radius and thickness of the arteriole, respectively.

Using Newton's second law of motion for this element, we have that

$$\Delta m \frac{d^2 R}{dt^2} = f_r + f_p \quad (30)$$

where  $\Delta m$  can be defined as

$$\Delta m = \rho_w 2\pi R_0 \Delta x h_0 \quad (31)$$

The tangential stress tensor component ( $\sigma_{\theta\theta}$ ) encompasses the passive elastic force, the viscous resistance force, and the active force (due to smooth muscle contraction), and is represented by the following equation:

$$\sigma_{\theta\theta} = \frac{E(F)}{1-\xi^2} \left[ \frac{R-R_0}{R_0} + c_1 \left( \frac{R-R_0}{R_0} \right)^2 \right] + \phi \frac{dR}{dt} + c_2 F_A \quad (32)$$

The first term describes the passive elastic force, the force exerted by the elastic lamina component of the cell wall, which is assumed to be weakly nonlinear with a quadratic correction.  $\phi$  is the constant of proportionality for the viscous component (the second term of the tensor).

The cellular calcium concentration and the subsequent development of myosin-actin crossbridges in SMCs is related by the cross-bridge phosphorylation and latch-state model of Hai and Murphy (1988). In their model, an elevation of calcium induces contraction through the formation of crossbridges between myosin and actin. Myosin can be in four possible states: free non-phosphorylated crossbridges [M], free phosphorylated crossbridges [Mp], attached

phosphorylated crossbridges [Amp], and attached dephosphorylated crossbridges [AM]. It is the fraction of myosin in the two attached states that determines the active stress, and hence contraction that can be effected in the arteriolar wall. Kudryashov and Chernyavskii (2008) define the active force on smooth muscle due to muscular tonus as  $k_2 F$  (where  $k_2$  is a constant and  $F$  is the concentration of contracting actin-myosin laments). For our model, we instead define  $F_A$  as the total fraction of attached crossbridges, i.e:

$$F_A = [\text{Amp}] + [\text{AM}] \quad (33)$$

We assume a value for the proportionality constant (which we denote as  $c_2$ ).

In  $\sigma_{\theta\theta}$  (Eq. (32)),  $E(F)$  represents Young's modulus, a measure of the "stiffness" of the cell wall material. We take Young's modulus to be an exponential function of  $F_A$ , as it is assumed that the cell wall material becomes increasingly (and exponentially) stiff when more crossbridges are in the attached state:

$$E(F) = E_0 + \varepsilon \exp\left(\frac{F_A}{F_{\max}}\right) \quad (34)$$

Here  $E_0$  is Young's modulus of inactive muscle (i.e.  $F_A=0$ ),  $F_{\max}$  is the maximum fraction of attached crossbridges and  $\varepsilon$  is an estimated stiffness coefficient.

Finally, defining the radius perturbation,  $\eta$ , as

$$R = R_0(1 + \eta) \quad (35)$$

we obtain the following differential equation for  $\eta$ :

$$\rho_w h_0 R_0 \frac{d^2 \eta}{dt^2} + \phi h_0 \frac{d\eta}{dt} + \frac{h_0 E(F)}{R_0(1-\xi^2)} [\eta + c_1 \eta^2] = \Delta p - \frac{h_0}{R_0} c_2 F \quad (36)$$

The second-order term in the perturbation DE is very small and only has an effect when looking at very small timescales. As our interest is confined to times much greater than those dominated by the second derivative, we therefore ignore it and solve the DE as a first-order equation instead.

## 2.7. Solution methodology

Neuronal activation was simulated by a release of glutamate and potassium into the synaptic cleft. This was achieved by assuming a smooth pulse (amplitude 0.5) for  $\rho$  (the fraction of bound glutamate receptors) and for the neuronal potassium flux ( $J_K$ ) for 60 s. All 23 differential equations (representing the entire neurovascular unit) were then solved using the solver RKSUITE, a robust mathematical solver written by Brankin et al. (1991). RKSUITE uses the embedded RK pair BS(4,5) method derived by Bogacki and Shampine (1996). It has a fifth-order accuracy and uses an adaptive step size method where the new step size ( $h_0$ ) is calculated using the algorithm:

$$h_0 = h_1 \left| \frac{\varepsilon_0}{\varepsilon_1} \right|^{1/p}$$

where  $p$  is the order, and  $h_1$  and  $\varepsilon_1$  are the previous step size and error, respectively.  $\varepsilon_0$  is the desired accuracy (or *relative error tolerance*) that we set to be  $1 \times 10^{-6}$ .

We also varied perivascular potassium concentration within the physiological range of values, and solved only the EC and SMC equations at each of these values. According to the experiment, a modest increase of potassium should induce vasodilation (Knot et al., 1996; McCarron and Halpern, 1990; Kuschinsky et al., 1972), but, paradoxically, a further increase in perivascular potassium should then cause vasoconstriction (Knot et al., 1996; Horiuchi et al., 2002). A similar effect (vasodilation followed by vasoconstriction) is observed in Girouard et al. (2010) when astrocyte cytosolic calcium is varied. We therefore manually

altered the astrocyte cytosolic calcium in our model equations so that we could compare to these experiments.

A parameter sensitivity analysis was also performed on the parameters  $R_{decay}$  (the rate of potassium clearance from the perivascular space) and  $eet_{shift}$  (the shift in the distribution of open BK channel states due to EET).

For simplicity, we consider one neurovascular unit only (that is, one synaptic space, one astrocyte and one arteriolar segment which will be represented as a set of identical smooth muscle cell-endothelial cell pairs heterogeneously coupled via IP3 and membrane voltage).

### 3. Results

Fig. 2 shows the response of modelled astrocyte variables to a 60-s neuronal activation (modelled as a 60-s pulse of potassium release and a pulse of partially bound Glu receptors ( $\rho = 0.5$ ) at  $t=0$ ). The increase in calcium in the cytosol, and the subsequent increase in EETs gate the BK channels in the astrocyte, causing a large increase in the open channel state probability (not shown) which then allows the release of a large potassium flux into the

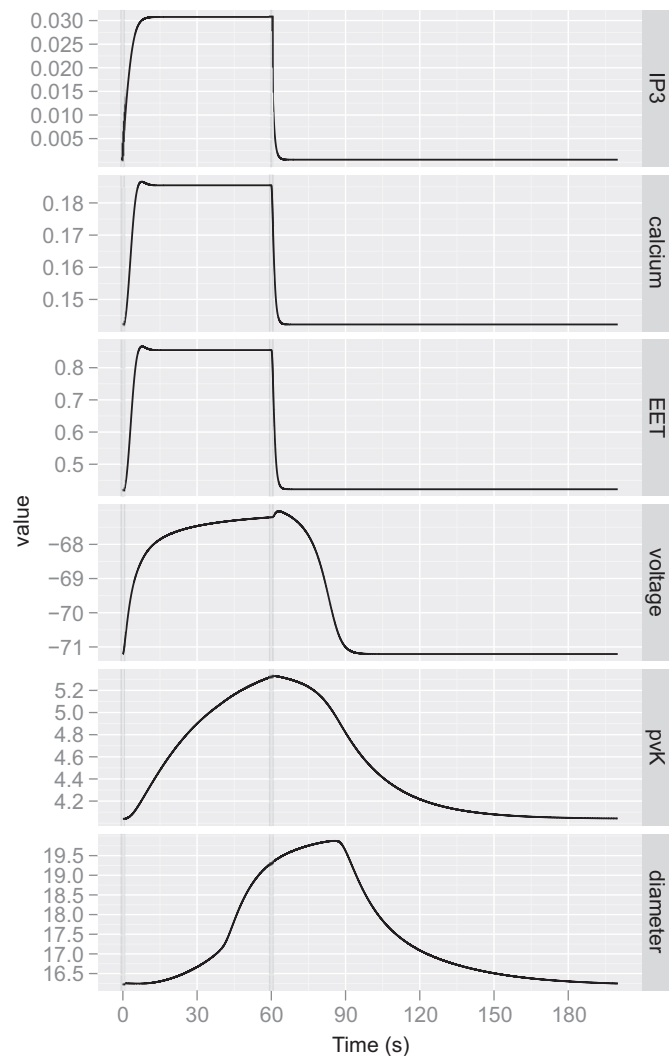


Fig. 2. Summary of the neurovascular response to a 60-s neuronal activation (shown here are the glutamate-induced increases in astrocytic  $IP_3$ , calcium and EET concentrations (mM), and their effect on the astrocyte voltage (mV), as well as subsequent increases in perivascular potassium, pvk (mM), and arteriolar diameter ( $\mu$ M)).

perivascular space (pvk). The astrocyte cell membrane undergoes a transient hyperpolarisation during this process (see voltage plot). The changes in perivascular potassium gate KIR channels on the vascular SMCs, concluding in the dilation of the arteriole (shown here in the “diameter” plot). It is difficult to see here whether or not EET lags calcium (as it is known to do). We can do a simple analysis to determine this (see Appendix B). If we assume that the increase in calcium after activation occurs in a linear fashion, we find that as long as  $1/k_{eet} < 1/V_{eet} + 1$  (which it is for our model) then EET will *always* lag calcium.

Fig. 3 compares the changes in SMC voltage at different perivascular potassium concentrations for our model and the experimental data of Edwards et al. (1988). This experimental data looks at proximal and distal segments of the middle cerebral artery (MCA).

Model simulations produce vasodilation at lower potassium concentrations and vasoconstriction at higher potassium concentrations (Fig. 4).

The trend seen in Fig. 3 can be best explained by observing the behaviour of  $v_{KIR}$  (the KIR Nernst reversal potential) and  $k$  (the

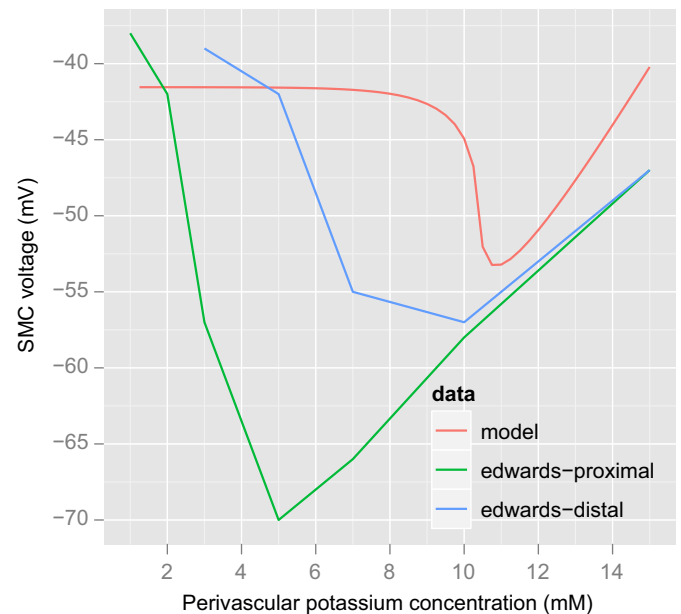


Fig. 3. Change in SMC voltage due to changing perivascular potassium concentration.

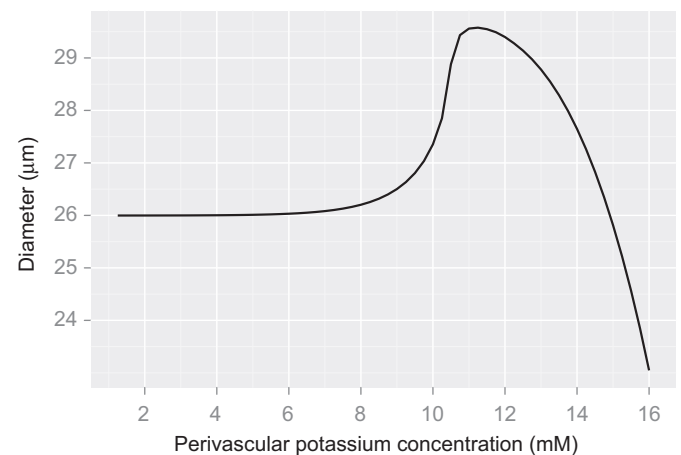


Fig. 4. Change in diameter due to changing perivascular potassium concentration.

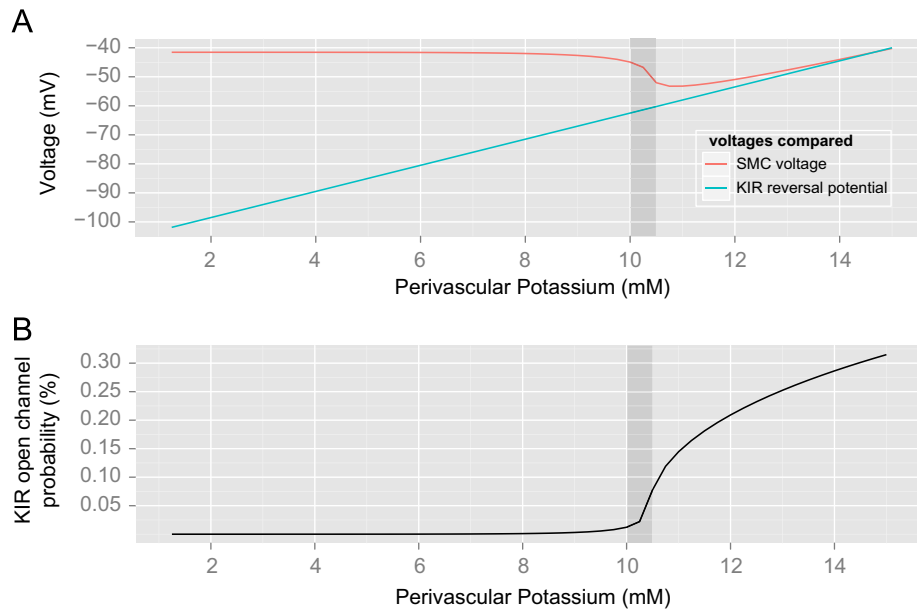


Fig. 5. Comparison of  $v_{KIR}$ ,  $k$  and SMC voltage relationships and perivascular potassium concentration.

fraction of open KIR channels) as potassium in the perivascular space increases, here shown in Fig. 5.

Manually adjusting the astrocyte cytosolic calcium concentration in our model gives a vasodilation at lower concentrations, and a vasoconstriction at higher concentrations (as per the experimental results of Girouard et al., 2010):

The parameter  $eet_{shift}$  determines to what degree the BK channel open probability is shifted when EET is produced in the astrocyte cytosol. Fig. 7 shows the effect that changing this parameter has on both the BK channel open probability (NPO) and the corresponding arteriolar radius when a 60-s neuronal activation is simulated.

Fig. 8 show the simulated changes in perivascular potassium (A) and radius (B) when different estimates for the “potassium clearance rates” were used for a 60-s neuronal activation. The longer potassium is allowed to remain in the perivascular space, the larger the dilation, the longer the vasodilation is sustained.

#### 4. Discussion

These results successfully support the hypothesis of a potassium- and EET-mediated exchange of information between arteriole and astrocyte (proposed by Filosa and Blanco, 2007). We show (Fig. 2) that a glutamate-induced calcium increase can gate BK channels in the astrocyte such that potassium is released into the perivascular space, causing a dilation. Our results support the hypotheses put forth by Higashimori et al. (2010): that EETs can act to modulate arterioles by acting in an autocrine manner.

The 15% increase in radius shown here is sufficient to change the resistance of the asymmetric binary tree of David et al. (2009) to the same degree that the previous phenomenological metabolic model did, making this present model a promising substitute.

Although we are able to achieve a radial change similar in magnitude to the flow changes seen in the experimental work of Shi et al. (2008) (approximately 15%), we are unable to emulate the speed of the response. Maximum flow changes are reached in less than 5 s from the onset of stimulation in the experiments of Shi et al. (2008), but only occur after 30 s in our model solution (due to the relatively slow uptake of the vasodilatory  $K^+$  by KIR channels in the SMCs). Shi et al. (2008) also show that blood flow

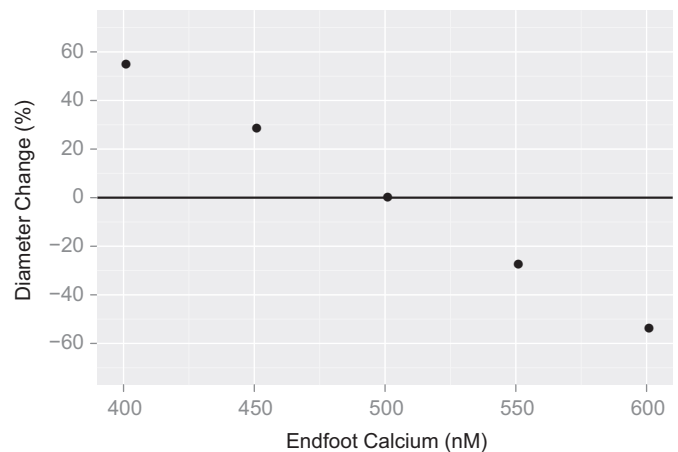


Fig. 6. Endfoot calcium determines both arteriolar constriction and dilation.

changes occur in the presence of EET antagonists, proving that EET mechanisms are certainly not the only mechanisms working to achieve successful functional hyperemia. A recent (and excellent) review on the regulation of blood flow via neurons and astrocytes by Attwell et al. (2010) describes these other mechanisms, including those involving  $O_2$  and NO. The arteriolar response to neuronal activation is therefore the sum of many such signals, some of which are faster than others. For example, it is known that NO is capable of diffusing rapidly over fairly long distances and is produced at many locations in the neurovascular unit (by neuronal NOS and endothelial NOS) meaning that its concentration at any given point is determined by the sum of all NO sources (Buerk, 2001). NO could therefore be better placed to elicit the initial, rapid blood flow response, whereas the EET/ $K^+$  signals are used to control dilations over more sustained activations. The dynamics of the  $O_2$  and NO pathways are therefore of great interest in the next stage of developing a model capable of the rapid metabolic autoregulation seen in experiment.

Fig. 3 compares the changes in SMC voltage at different perivascular potassium concentrations for our model and the experimental data of Edwards et al. (1988). This experimental data looks at proximal and distal segments of the middle cerebral

artery (MCA). The same general trend can be seen in both the model and experimental data, that is: that increasing the perivascular potassium concentration causes a hyperpolarisation, and then a depolarisation in SMC membrane potential. However, there exists a difference between the membrane potential of the SMC at the physiological value of potassium (3 mM) between model and even between different experimental data (as is seen as an offset between each curve). This is unsurprising as it is known that there is a variable distribution of resting membrane potentials (Jiang et al., 2001; Siegl et al., 2005) and ion channel expression (Quayle et al., 1996) along the vasculature, just as there is very different structural and signalling specialisations

underlying how blood flow is locally regulated at different levels of the tree (Borisova et al., 2009).

The paradoxical but experimentally observed effect where increased potassium causes first an increase and then a decrease in radius is successfully simulated (Fig. 4). The mechanisms behind this phenomena have never been fully elucidated, although it has previously been attributed to the interactions of SMC  $\text{Na}^+ - \text{K}^+$  pumps and KIR channel currents (McCarron and Halpern, 1990; Quinn et al., 2000). Our investigations into the cause of this trend (Fig. 5A and B) point to the interactions between the fraction of open KIR channels ( $k$ ) and the changing value of the potassium-dependent resting potential of the KIR

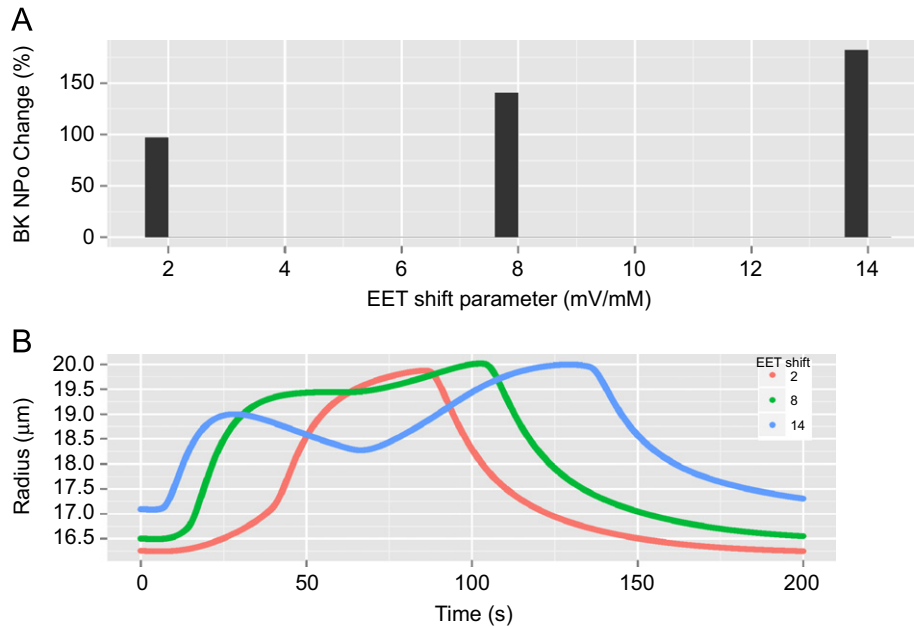


Fig. 7. Sensitivity analysis for parameter  $eet\_shift$ .

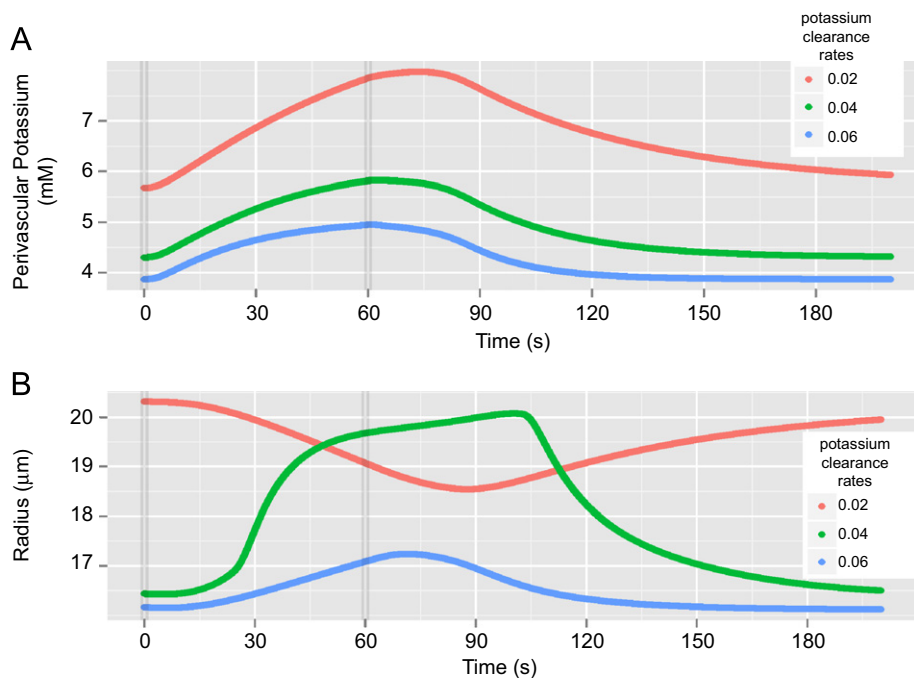


Fig. 8. Model perivascular potassium concentration (A) and radius (B) changes for various “potassium clearance rates”.

channel ( $v_{KIR}$ ). These peculiar interactions cause the KIR channels to exhibit an “all-or-nothing” effect. The KIR channels will always attempt to rectify the SMC voltage to  $v_{KIR}$  by passing potassium in or out of the cell. The size of the potassium current passed is the product of the voltage “driving force” (the difference between the SMC voltage and the reversal potential) and the fraction of open KIR channels (Eq. (21)). Fig. 5A shows that the driving force is very large at lower concentrations of potassium, and the SMC voltage should attempt to hyperpolarise so as to rectify to the reversal potential. However, because there is only a very small fraction of channels open at more depolarised voltages (Fig. 5B), only very small fluxes of potassium can pass through the KIR channels. The small fluxes of potassium leaving through the KIR channels do eventually cause the SMC voltage to hyperpolarise to the critical “gating” voltage (approximately  $-45$  mV) at which KIR channels open rapidly. The rapid increase in channel openings allows large fluxes of potassium to exit via the KIR channels; rapidly hyperpolarising the SMC membrane. The SMC membrane potential then depolarises at higher potassium concentrations to rectify to the changing  $v_{KIR}$  (Fig. 5A).

Another paradoxical effect (this time: vasodilation followed by vasoconstriction with increasing endfoot calcium concentrations) seen in the work of Girouard et al. (2010) is successfully emulated in our model simulations also (Fig. 6). The cellular mechanisms behind this experimental phenomena can perhaps be explained now that we have an appreciation of the SMC KIR channel dynamics (Fig. 5). Endfoot calcium begins the vasomodulatory signal by determining BK release of potassium and SMC KIR channels then “read” this signal and determine whether to constrict or dilate, and by how much. Therefore, these model investigations, like the experimental results of Girouard et al. (2010), support the concept that endfoot BK and smooth muscle KIR channels act in series, together forming a signalling module.

The parameter  $eet_{shift}$  determines to what degree the BK channel open probability distribution is shifted when EET is produced in the astrocyte cytosol. Fig. 7A and B shows the effect that changing this parameter has on the BK channel open probability (NPo), and the arteriolar radius, respectively. The value for  $eet_{shift}$  that we use in our model (2 mV/mM) gives a NPo shift of close to 100% (the approximate change seen for EET application in Lu et al., 2001), but altering this parameter can cause NPo changes greater than this (NPo changes seen in Lu et al., 2001 due to the application of the EET-metabolite DHET reaches much higher values). The degree of the shift in the BK channel distribution can cause completely different behaviour in terms of the arteriolar radius (dilations only or dilations with transient constrictions), due to their influence on potassium levels in the perivascular space. Transient constrictions occur when the perivascular potassium concentration exceeds approximately 11 mM (the concentration where arteriolar behaviour changes—see Fig. 4) Note that there is also a quicker response when  $eet_{shift}$  is larger.

Fig. 8B shows that the potassium clearance rate determines what sort of vessel response is achieved (dilation or constriction), as well as the size of that response (large or small). Furthermore, the potassium clearance rates can affect the value of the resting (basal) arteriolar tone. These results highlight the potential importance of controlling not only the release of potassium into the perivascular space but also the clearance of potassium from it—if potassium is not cleared at the appropriate rate, arterioles may exhibit the incorrect behaviour (constrict instead of dilate or not dilate to a large enough degree or dilate longer than is necessary for efficient blood flow autoregulation). This current model does not include the important physiological mechanisms involved in potassium clearance (i.e. “potassium buffering” via VRAs).

## 5. Conclusions and future work

Our mathematical model simulates neurovascular coupling using EET and  $K^+$  as the major signalling pathways. Constructing a model of sufficient physiological complexity has allowed us to investigate the causes of experimentally observed observations, such as the effect where increased perivascular potassium causes first an arteriolar dilation and then a constriction. This project highlights the fact that mathematical modelling can be used as a tool to understand biological processes in a way that physical experiment cannot always do.

We were able to achieve vasodilations (and vasoconstrictions) similar in magnitude to those seen in experiment (Girouard et al., 2010; Shi et al., 2008). We believe that the introduction of other known major neurovascular coupling pathways (especially those of  $O_2$  and NO) may be capable of producing a response closer to the physiological speed required. We also intend to extend this model into complex networks of neurovascular units coupled into an asymmetric binary tree representing significant sections of the cerebrovasculature, so that whole brain changes can be observed.

## Acknowledgements

This group would like to thank the Van der Veer Institute for Parkinson's and Brain Research and the University of Canterbury for providing PhD funding for this project, and the Canterbury Medical Research Foundation for providing MR scanning funding. We would also like to thank BlueFern—New Zealand's supercomputing and services facility for research and development—for their advice and help on the Brain Project.

## Appendix A. Model parameters

Parameters used in this model are given in Tables A.1–A.4. See text for parameter descriptions.

See Section 2.5 and Koenigsberger et al. (2006) for parameters used in the SMC and EC equations.

**Table A.1**  
Parameters for the astrocyte equations.

Parameter	Value	Source
$B_{cyt}$	0.0244	Bennett et al. (2008)
$VR_{ERcyt}$	0.185	Ullah et al. (2006)
$J_{max}$	2880 $\mu\text{M s}^{-1}$	Bennett et al. (2008)
$K_i$	0.03 $\mu\text{M}$	Bennett et al. (2008)
$K_{act}$	0.17 $\mu\text{M}$	Bennett et al. (2008)
$P_L$	5.2 $\mu\text{M}$	Lemon et al. (2003)
$V_{max}$	20 $\mu\text{M s}^{-1}$	Bennett et al. (2008)
$k_{pump}$	0.24 $\mu\text{M}$	Bennett et al. (2008)
$k_{on}$	2 $\mu\text{M s}^{-1}$	Bennett et al. (2008)
$k_{inh}$	0.1 $\mu\text{M}$	Bennett et al. (2008)
$r_h$	4.8 $\mu\text{M}$	Bennett et al. (2008)
$k_{deg}$	1.25 $\text{s}^{-1}$	Bennett et al. (2008)
$\delta$	$1.235 \times 10^{-3} \mu\text{M}$	Bennett et al. (2008)
$K_G$	8.82 $\mu\text{M}$	Bennett et al. (2008)
$V_{eet}$	72 $\mu\text{M}$	Bennett et al. (2008)
$k_{eet}$	7.2 $\mu\text{M}$	Estimation
$C_{k,min}$	0.1 $\mu\text{M}$	Bennett et al. (2008)
$J_{naK_{max}}$	1 $\text{mMs}^{-1}$	Estimation
$KKO_a$	1.5 mM	Østby et al. (2009)
$NaI_a$	15 mM	Østby et al. (2009)
$KNaI_a$	10 mM	Østby et al. (2009)
$k_{pmin}$	3 mM	Kofuji and Newman (2004)

**Table A.2**

Parameters for the astrocyte ion channel equations.

Parameter	Value	Source
$g_{leak_k}$	78.54 pS	Gonzalez-Fernandez and Ermentrout (1994)
$v_{leak_k}$	-70 mV	Gonzalez-Fernandez and Ermentrout (1994)
$g_{BK_k}$	13 854 pS	Estimation
$v_{BK_k}$	-95 mV	Gonzalez-Fernandez and Ermentrout (1994)
$eet_{shift}$	2 mV $\mu\text{M}^{-1}$	Lu et al. (2001)
$\psi_n$	2.664 s <sup>-1</sup>	Gonzalez-Fernandez and Ermentrout (1994)
$v_4$	14.5 mV	Gonzalez-Fernandez and Ermentrout (1994)
$v_5$	8 mV	Gonzalez-Fernandez and Ermentrout (1994)
$v_6$	-15 mV	Gonzalez-Fernandez and Ermentrout (1994)
$\text{Ca}_3$	400 nM	Gonzalez-Fernandez and Ermentrout (1994)
$\text{Ca}_4$	150 nM	Gonzalez-Fernandez and Ermentrout (1994)

**Table A.3**

Parameters for perivascular space equations.

Parameter	Value	Source
$VR_{pa}$	0.0005	Estimate—Matyash and Kettenmann (2010)
$VR_{ps}$	0.1	Estimate—Stensaas (1975)
$R_{decay}$	0.05 s <sup>-1</sup>	Estimation

**Table A.4**

Parameters used in muscle mechanics equations.

Parameter	Value	Source
$R_0$	10 $\mu\text{m}$	Lauwers et al. (2008)
$h_0$	4 $\mu\text{m}$	Lauwers et al. (2008)
$\rho_w$	1100 kg m <sup>-3</sup>	Kudryashov and Chernyavskii (2008)
$\zeta$	0.5	Kudryashov and Chernyavskii (2008)
$c_1$	0.015	Kudryashov and Chernyavskii (2008)
$\phi$	750 $\times 10^6$ Pa $\mu\text{m}^{-1}$ s	Kudryashov and Chernyavskii (2008)
$c_2$	50 000 Pa	Gore and Davis (1984)
$E_0$	15 000 Pa	Kudryashov and Chernyavskii (2008)
$\varepsilon$	1500 Pa	Estimation
$F_{max}$	0.8	Hai and Murphy (1988)
$\Delta_p$	4000 Pa	Lauwers et al. (2008)

## Appendix B. Analysis of EET increase with respect to a calcium input function

We show below an argument to support the hypothesis that [EET] does increase “after”  $\text{Ca}^{2+}$ . The differential equation for [EET] (denoted by  $\phi(t)$ ) is given by

$$\frac{d\phi}{dt} = V(c(t) - c_{min}) - k\phi \quad (\text{B.1})$$

We assume that  $c(t) - c_{min} = C(t)$  with  $C(0) = 0$ . then

$$\frac{d\phi}{dt} + k\phi = VC(t) \quad (\text{B.2})$$

a solution to this is easily formed

$$e^{kt}\phi(t)|_0^t = V \int_0^t C(\tau)e^{k\tau} d\tau \quad (\text{B.3})$$

However we do not know the exact formulation of  $C(t)$ . For small values of time,  $t$  we assume that  $C(t) \approx \alpha t$  then

$$\phi(t) = [\phi(0) + \gamma(t)]e^{-kt} \quad (\text{B.4})$$

with

$$\gamma(t) = V \int_0^t \alpha \tau e^{k\tau} d\tau \quad (\text{B.5})$$

integrating  $\gamma(t)$  by parts we have that

$$\gamma(t) = \alpha V \left[ \frac{\tau}{k} e^{k\tau} - \int_0^t e^{k\tau} d\tau \right] \quad (\text{B.6})$$

$$\gamma(t) = \frac{\alpha V}{k} [e^{kt}(t-1) + 1] \quad (\text{B.7})$$

so

$$\phi(t) = \frac{\alpha V}{k}(t-1) + \frac{\alpha V}{k}e^{-kt} \quad (\text{B.8})$$

using a Taylor expansion for  $e^{-kt}$  we have that

$$\phi(t) = \alpha Vt \left[ \frac{1}{k} - 1 \right] + O(kt^2) \quad (\text{B.9})$$

clearly  $\phi(t)$  increase hence  $(1/k-1) > 0$  since all  $\alpha$ ,  $V$  and  $k$  are  $> 0$ . If  $\phi(t)$  is to increase at a slower rate than  $\text{Ca}^{2+}$  then

$$V \left[ \frac{1}{k} - 1 \right] < 1 \quad (\text{B.10})$$

$$\frac{1}{k} < \frac{1}{V} + 1 \quad (\text{B.11})$$

So by choosing either  $V$  or  $k$  the other is completely defined for [EET] to lag  $[\text{Ca}^{2+}]$ . If we choose  $C(t) = \tilde{c}H(t)$  then

$$\phi(t) = \frac{V}{k} [1 - e^{-kt}] \Rightarrow \phi(t) \approx Vt \quad (\text{B.12})$$

for small  $t$  and therefore always lags  $[\text{Ca}^{2+}]$ .

## References

- Attwell, D., Buchan, A.M., Charpak, S., Lauritzen, M., Macvicar, B.A., Newman, E.A., 2010. Glial and neuronal control of brain blood flow. *Nature* 468 (7321), 232–243. doi:10.1038/nature09613.
- Bennett, M.R., Farnell, L., Gibson, W.G., 2008. Origins of blood volume change due to glutamatergic synaptic activity at astrocytes abutting on arteriolar smooth muscle cells. *J. Theor. Biol.* 250 (1), 172–185. doi:10.1016/j.jtbi.2007.08.024.
- Bogacki, P., Shampine, L.F., 1996. An efficient Runge–Kutta (4,5) pair. *Comput. Math. Appl.* 32 (6), 15–28.
- Borisova, L., Wray, S., Eisner, D.A., Burdyga, T., 2009. How structure, Ca signals, and cellular communications underlie function in precapillary arterioles. *Circ. Res.* 105 (8), 803–810. doi:10.1161/CIRCRESAHA.109.202960.
- Brankin, R.W., Gladwell, I., Shampine, L.F., 1991. Rksuite Release 1.0, Technical Report.
- Buerk, D.G., 2001. Can we model nitric oxide biotransport? A survey of mathematical models for a simple diatomic molecule with surprisingly complex biological activities. *Annu. Rev. Biomed. Eng.* 3, 109–143. doi:10.1146/annurev.bieng.3.1.109.
- Cameron, I.R., Caronna, J., 1976. The effect of local changes in potassium and bicarbonate concentration on hypothalamic blood flow in the rabbit. *J. Physiol.* 262 (2), 415–430.
- Carmignoto, G., Pasti, L., Pozzan, T., 1998. On the role of voltage-dependent calcium channels in calcium signaling of astrocytes in situ. *J. Neurosci.* 18 (12), 4637–4645.
- Chen, K.C., Nicholson, C., 2000. Spatial buffering of potassium ions in brain extracellular space. *Biophys. J.* 78 (6), 2776–2797. doi:10.1016/S0006-3495(00)76822-6.
- Chrissobolis, S., Ziogas, J., Chu, Y., Faraci, F.M., Sobey, C.G., 2000. Role of inwardly rectifying K(+) channels in K(+)-induced cerebral vasodilatation in vivo. *Am. J. Physiol. Heart Circ. Physiol.* 279 (6), H2704–H2712.
- David, T., Alzaidi, S., Farr, H., 2009. Coupled autoregulation models in the cerebrovasculature. *J. Eng. Math.* 64 (4), 403–415. doi:10.1007/s10665-009-9274-2.
- Edwards, F.R., Hirst, G.D., Silverberg, G.D., 1988. Inward rectification in rat cerebral arterioles: involvement of potassium ions in autoregulation. *J. Physiol.* 404, 455–466.
- Ehrenstein, G., Lecar, H., 1977. Electrically gated ionic channels in lipid bilayers. *Q. Rev. Biophys.* 10 (1), 1–34.
- Filosa, J.A., Blanco, V.M., 2007. Neurovascular coupling in the mammalian brain. *Exp. Physiol.* 92 (4), 641–646. doi:10.1113/expphysiol.2006.036368.
- Filosa, J.A., Bonev, A.D., Straub, S.V., Meredith, A.L., Wilkerson, M.K., Aldrich, R.W., Nelson, M.T., 2006. Local potassium signaling couples neuronal activity to vasodilation in the brain. *Nat. Neurosci.* 9 (11), 1397–1403. doi:10.1038/nn1779.
- Girouard, H., Iadecola, C., 2006. Neurovascular coupling in the normal brain and in hypertension, stroke, and Alzheimer disease. *J. Appl. Physiol.* 100 (1), 328–335. doi:10.1152/jappphysiol.00966.2005.

- Girouard, H., Bonev, A.D., Hannah, R.M., Meredith, A., Aldrich, R.W., Nelson, M.T., 2010. Astrocytic endfoot  $Ca^{2+}$  and BK channels determine both arteriolar dilation and constriction. *Proc. Natl. Acad. Sci. USA* 107 (8), 3811–3816. doi:10.1073/pnas.0914722107.
- Golding, E.M., Steenberg, M.L., Johnson, T.D., Bryan Jr., R.M., 2000. The effects of potassium on the rat middle cerebral artery. *Brain Res.* 880 (1–2), 159–166.
- Gonzalez-Fernandez, J.M., Ermentrout, B., 1994. On the origin and dynamics of the vasomotion of small arteries. *Math. Biosci.* 119 (2), 127–167.
- Gore, R.W., Davis, M.J., 1984. Mechanics of smooth muscle in isolated single microvessels. *Ann. Biomed. Eng.* 12 (5), 511–520.
- Hai, C.M., Murphy, R.A., 1988. Cross-bridge phosphorylation and regulation of latch state in smooth muscle. *Am. J. Physiol.* 254 (1 Pt 1), C99–C106.
- Higashi, K., Fujita, A., Inanobe, A., Tanemoto, M., Doi, K., Kubo, T., Kurachi, Y., 2001. An inwardly rectifying  $K^{+}$  channel *kir41*, expressed in astrocytes surrounds synapses and blood vessels in brain. *Am. J. Physiol. Cell Physiol.* 281 (3), C922–C931.
- Higashimori, H., Blanco, V.M., Tuniki, V.R., Falck, J.R., Filosa, J.A., 2010. Role of epoxyeicosatrienoic acids as autocrine metabolites in glutamate-mediated  $K^{+}$  signaling in perivascular astrocytes. *Am. J. Physiol. Cell Physiol.* 299 (5), C1068–C1078. doi:10.1152/ajpcell.00225.2010.
- Horiuchi, T., Dietrich, H.H., Hongo, K., Dacey Jr., R.G., 2002. Mechanism of extracellular  $K^{+}$ -induced local and conducted responses in cerebral penetrating arterioles. *Stroke* 33 (11), 2692–2699.
- Iadecola, C., 2004. Neurovascular regulation in the normal brain and in Alzheimer's disease. *Nat. Rev. Neurosci.* 5 (5), 347–360. doi:10.1038/nrn1387.
- Jiang, Z.G., Si, J.Q., Lasarev, M.R., Nuttall, A.L., 2001. Two resting potential levels regulated by the inward-rectifier potassium channel in the guinea-pig spiral modiolar artery. *J. Physiol.* 537 (Pt 3), 829–842.
- Johnson, T.D., Marrelli, S.P., Steenberg, M.L., Childres, W.F., Bryan Jr., R.M., 1998. Inward rectifier potassium channels in the rat middle cerebral artery. *Am. J. Physiol.* 274 (2 Pt 2), R541–R547.
- Knot, H.J., Zimmermann, P.A., Nelson, M.T., 1996. Extracellular  $K^{+}$ -induced hyperpolarizations and dilatations of rat coronary and cerebral arteries involve inward rectifier  $K^{+}$  channels. *J. Physiol.* 492 (Pt 2), 419–430.
- Koenigsberger, M., Sausser, R., Beny, J.-L., Meister, J.-J., 2006. Effects of arterial wall stress on vasomotion. *Biophys. J.* 91 (5), 1663–1674. doi:10.1529/biophysj.106.083311.
- Kofuji, P., Newman, E.A., 2004. Potassium buffering in the central nervous system. *Neuroscience* 129 (4), 1045–1056. doi:10.1016/j.neuroscience.2004.06.008.
- Kudryashov, N., Chernyavskii, I., 2008. Numerical simulation of the process of autoregulation of the arterial blood flow. *Fluid Dyn.* 43 (1), 32–48. doi.org/10.1134/s10697-008-1005-2.
- Kurachi, Y., 1985. Voltage-dependent activation of the inward-rectifier potassium channel in the ventricular cell membrane of guinea-pig heart. *J. Physiol.* 366, 365–385.
- Kuschinsky, W., Wahl, M., Bosse, O., Thurau, K., 1972. Perivascular potassium and pH as determinants of local pial arterial diameter in cats. A microapplication study. *Circ. Res.* 31 (2), 240–247.
- Lauwers, F., Cassot, F., Lauwers-Cances, V., Puwanarajah, P., Duvernoy, H., 2008. Morphometry of the human cerebral cortex microcirculation: general characteristics and space-related profiles. *Neuroimage* 39 (3), 936–948. doi:10.1016/j.neuroimage.2007.09.024.
- Lemon, G., Gibson, W.G., Bennett, M.R., 2003. Metabotropic receptor activation, desensitization and sequestration—i: modelling calcium and inositol 1,4,5-trisphosphate dynamics following receptor activation. *J. Theor. Biol.* 223 (1), 93–111.
- Lu, T., Katakam, P.V., VanRollins, M., Weintraub, N.L., Spector, A.A., Lee, H.C., 2001. Dihydroxyeicosatrienoic acids are potent activators of  $Ca^{2+}$ -activated  $K^{+}$  channels in isolated rat coronary arterial myocytes. *J. Physiol.* 534 (Pt 3), 651–667.
- Matyash, V., Kettenmann, H., 2010. Heterogeneity in astrocyte morphology and physiology. *Brain Res. Rev.* 63 (1–2), 2–10. doi:10.1016/j.brainresrev.2009.12.001.
- McCarron, J.G., Halpern, W., 1990. Potassium dilates rat cerebral arteries by two independent mechanisms. *Am. J. Physiol.* 259 (3 Pt 2), H902–H908.
- Metea, M.R., Kofuji, P., Newman, E.A., 2007. Neurovascular coupling is not mediated by potassium siphoning from glial cells. *J. Neurosci.* 27 (10), 2468–2471. doi:10.1523/jneurosci.3204-06.2007.
- Morris, C., Lecar, H., 1981. Voltage oscillations in the barnacle giant muscle fiber. *Biophys. J.* 35 (1), 193–213. doi:10.1016/S0006-3495(81)84782-0.
- Nakahata, K., Kinoshita, H., Tokinaga, Y., Ishida, Y., Kimoto, Y., Dojo, M., Mizumoto, K., Ogawa, K., Hatano, Y., 2006. Vasodilation mediated by inward rectifier  $K^{+}$  channels in cerebral microvessels of hypertensive and normotensive rats. *Anesth. Analg.* 102 (2), 571–576. doi:10.1213/01.ane.0000194303.00844.5e.
- Nystoriak, M.A., O'Connor, K.P., Sonkusare, S.K., Brayden, J.E., Nelson, M.T., Wellman, G.C., 2011. Fundamental increase in pressure-dependent constriction of brain parenchymal arterioles from subarachnoid hemorrhage model rats due to membrane depolarization. *Am. J. Physiol. Heart Circ. Physiol.* 300 (3), H803–H812. doi:10.1152/ajpheart.00760.2010.
- Østby, I., Øyehaug, L., Einevoll, G.T., Nagelhus, E.A., Plahte, E., Zeuthen, T., Lloyd, C.M., Ottersen, O.P., Omholt, S.W., 2009. Astrocytic mechanisms explaining neural-activity-induced shrinkage of extraneuronal space. *PLoS Comput. Biol.* 5 (1), e1000272. doi:10.1371/journal.pcbi.1000272.
- Paulson, O.B., Newman, E.A., 1987. Does the release of potassium from astrocyte endfeet regulate cerebral blood flow? *Science* 237 (4817), 896–898.
- Price, D.L., Ludwig, J.W., Mi, H., Schwarz, T.L., Ellisman, M.H., 2002. Distribution of rSlo  $Ca^{2+}$ -activated  $K^{+}$  channels in rat astrocyte perivascular endfeet. *Brain Res.* 956 (2), 183–193.
- Quayle, J.M., Dart, C., Standen, N.B., 1996. The properties and distribution of inward rectifier potassium currents in pig coronary arterial smooth muscle. *J. Physiol.* 494 (Pt 3), 715–726.
- Quayle, J.M., Nelson, M.T., Standen, N.B., 1997. Atp-sensitive and inwardly rectifying potassium channels in smooth muscle. *Physiol. Rev.* 77 (4), 1165–1232.
- Quinn, K., Guibert, C., Beech, D.J., 2000. Sodium–potassium-ATPase electrogenicity in cerebral precapillary arterioles. *Am. J. Physiol. Heart Circ. Physiol.* 279 (1), H351–H360.
- Setoguchi, M., Ohya, Y., Abe, I., Fujishima, M., 1997. Stretch-activated whole-cell currents in smooth muscle cells from mesenteric resistance artery of guinea-pig. *J. Physiol.* 501 (Pt 2), 343–353.
- Shi, Y., Liu, X., Gebremedhin, D., Falck, J.R., Harder, D.R., Koehler, R.C., 2008. Interaction of mechanisms involving epoxyeicosatrienoic acids, adenosine receptors, and metabotropic glutamate receptors in neurovascular coupling in rat whisker barrel cortex. *J. Cereb. Blood Flow Metab.* 28 (1), 111–125. doi:10.1038/sj.jcbfm.9600511.
- Siegl, D., Koeppe, M., Wölfle, S.E., Pohl, U., de Wit, C., 2005. Myoendothelial coupling is not prominent in arterioles within the mouse cremaster microcirculation in vivo. *Circ. Res.* 97 (8), 781–788. doi:10.1161/01.RES.0000186193.22438.6c.
- Stensaas, L.J., 1975. Pericytes and perivascular microglial cells in the basal forebrain of the neonatal rabbit. *Cell Tissue Res.* 158 (4), 517–541.
- Ullah, G., Jung, P., Cornell-Bell, A.H., 2006. Anti-phase calcium oscillations in astrocytes via inositol (1, 4, 5)-trisphosphate regeneration. *Cell Calcium* 39 (3), 197–208. doi:10.1016/j.ceca.2005.10.009.
- Xu, G., Antuono, P.G., Jones, J., Xu, Y., Wu, G., Ward, D., Li, S.-J., 2007. Perfusion fMRI detects deficits in regional CBF during memory-encoding tasks in MCI subjects. *Neurology* 69 (17), 1650–1656. doi:10.1212/01.wnl.0000296941.06685.22.
- Zhou, M., Kimelberg, H.K., 2000. Freshly isolated astrocytes from rat hippocampus show two distinct current patterns and different  $[K^{+}]_o$  uptake capabilities. *J. Neurophysiol.* 84 (6), 2746–2757.